Cafarelli *et al.*
Smart Construction and Sustainable Cities (2024) 2:5
https://doi.org/10.1007/s44268-024-00026-6

Smart Construction and Sustainable Cities

RESEARCH Open Access

Failure-mode scale transitions in RC and PC beams

Renato Cafarelli[1*], Federico Accornero[2] and Alberto Carpinteri[1,2]

Abstract

Current design Standards for reinforced concrete beams prescribe to respect a minimum, ρ_{min}, and a maximum, ρ_{max}, reinforcement ratio in the design of structures. Below ρ_{min} a brittle failure due to unstable crack propagation is expected. On the other hand, for $\rho > \rho_{max}$ a brittle failure due to concrete crushing is obtained. In this framework, a reinforced concrete element with $\rho_{min} < \rho < \rho_{max}$ presents yielded steel at Ultimate Limite State (ULS) with a stable behaviour and no catastrophic loss of bearing capacity. Design Standards define ρ_{min} and ρ_{max} limits on the basis of the Bernoulli's hypothesis of plane sections, and completely disregard size-scale effects. Within the present paper, Dimensional Analysis is used to determine the Brittleness Numbers that govern the behaviour of reinforced concrete (RC) as well as of prestressed reinforced concrete (PC) beams. Therefore, parametric analyses carried out by means of the Cohesive/Overlapping Crack Model (COCM) are used to study the ductile-to-brittle transitions in RC and PC beams, and to highlight the size-scale dependency of the two above-mentioned reinforcement limits.

Keywords Reinforced concrete, Cracking, Crushing, Minimum reinforcement, Maximum reinforcement, Scale effects

1 Introduction

Design Standards for reinforced concrete (RC) and prestressed reinforced concrete (PC) beams are based on the following four assumptions:

- the tensile strength of concrete may be neglected;
- the constitutive law for concrete in compression is defined in a σ-ε diagram;
- the constitutive law for steel is defined in a σ-ε diagram;
- plain sections remain plane after deformation.

The first assumption is due to the low tension strength of the concrete matrix: since the tension strength, σ_t, is one order of magnitude lower than the compression stength, σ_c, it may be neglected for practical reasons.

In Fig. 1, stress–strain curves in compression for several concrete grades according to Model Code 2010 [21] are reported. It may be observed that for high strain levels the curves are markedly nonlinear, suggesting that the actual stress distribution in the compressed zone of a RC beam is a function of the loading stage. Therefore, the stress may be considered linear only for low load levels. On the other hand, when the flexural strength of the section is reached, the stress distribution becomes nonlinear and may be described as a function of the parameters k_1, k_2, and k_3, as reported in Fig. 2. In this framework, with the introduction of Limit Design for RC beams (1937), Whitney [38] introduced an equivalent stress block to simplify the calculations: the actual distribution of the stress within the compressed zone may be substituted by an equivalent rectangular stress block having a width of $\eta\sigma_c$ and a depth of βx, x being the neutral axis depth, and β, $\eta \leq 1$ (Fig. 2). The assumption introduced by Whitney [38] has been widely accepted and calculation models

*Correspondence:
Renato Cafarelli
renato.cafarelli@polito.it
[1] Department of Structural, Geotechnical, and Building Engineering, Politecnico Di Torino, C.So Duca Degli Abruzzi 24, 10129 Turin, Italy
[2] Department of Civil Engineering and Smart Cities, Shantou University, Shantou, China

Springer

© The Author(s) 2024. **Open Access** This article is licensed under a Creative Commons Attribution 4.0 International License, which permits use, sharing, adaptation, distribution and reproduction in any medium or format, as long as you give appropriate credit to the original author(s) and the source, provide a link to the Creative Commons licence, and indicate if changes were made. The images or other third party material in this article are included in the article's Creative Commons licence, unless indicated otherwise in a credit line to the material. If material is not included in the article's Creative Commons licence and your intended use is not permitted by statutory regulation or exceeds the permitted use, you will need to obtain permission directly from the copyright holder. To view a copy of this licence, visit http://creativecommons.org/licenses/by/4.0/.

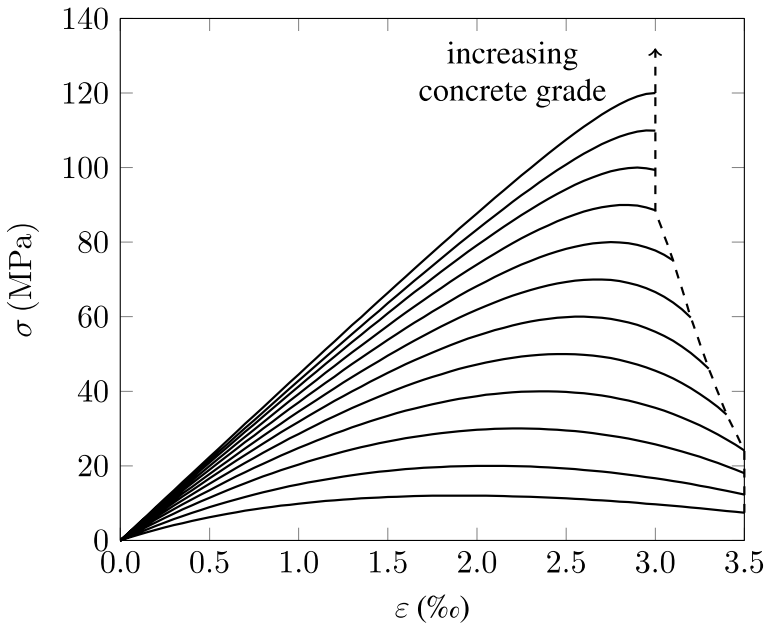

Fig. 1 Constitutive laws for concrete in compression [21]

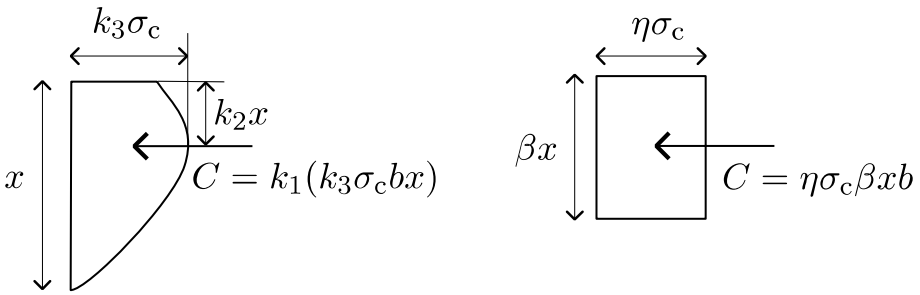

Fig. 2 Stress distribution for concrete in compression and equivalent stress block

included in current Standards are based on the equivalent stress block of Fig. 2.

The elastic-perfectly plastic constitutive law reported in Fig. 3 is usually adopted for steel reinforcement: since a possible strain-hardening implies an increase in the load bearing capacity, it may be neglected in order to simplify calculations.

The last hypothesis introduced above is known as Bernoulli's principle and implies that the strain in concrete and in the steel reinforcement is proportional to the distance from the neutral axis. Generally, this assumption is reliable at all stages of loading up to failure, if good bond between the reinforcement and the surrounding concrete exists. Nevertheless, in the zone close to a crack this assumption is not completely respected since a slip between the concrete matrix and the reinforcement always occurs.

Based on the hypotheses introduced above, Standards distinguish three different types of failure for beams in bending: *flexural failure*, *balanced failure* and *crushing failure*. In the case of a *flexural failure*, steel is yielded at ULS and if the axial force $N=0$, the depth, x, of the neutral axis of a rectangular cross-section may be found as:

$$x = \frac{A_s\sigma_y}{\eta\beta\sigma_c b}, \tag{1}$$

and the corresponding ultimate bending moment, M_u, as

$$M_u = \Phi\sigma_y A_s d\left(1 - 0.5\frac{A_s\sigma_y}{\eta\beta\sigma_c bd}\right), \tag{2}$$

d being the effective beam depth, and $\Phi \leq 1$ a strength reduction factor. Although Standards neglect the tension strength of concrete, they require to design RC elements providing a reinforcement percentage higher than a lower

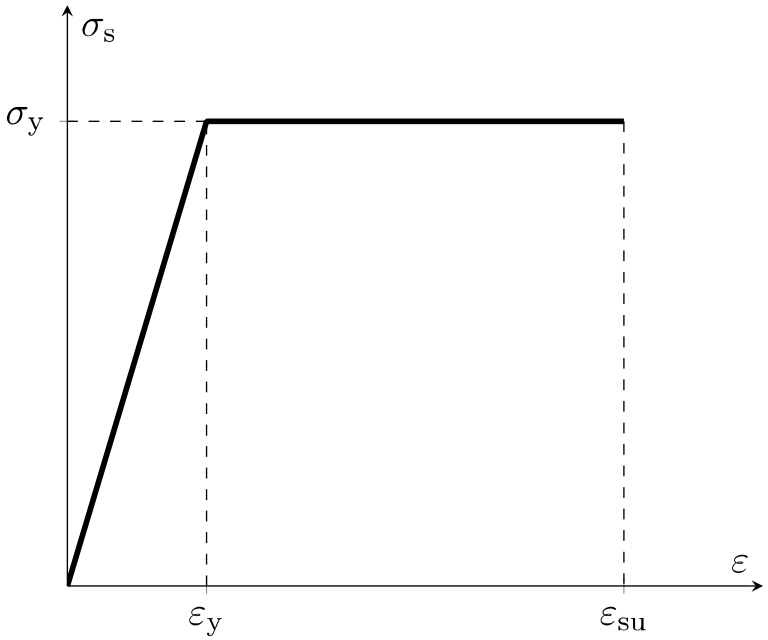

Fig. 3 Constitutive law for steel

bound, ρ_{min}, in order to avoid hyperstrength phenomena. In this framework, by neglecting in (2) the second term in brackets and by equalling $M_u = M_{cr}$, M_{cr} being the cracking bending moment, it is possible to obtain the minimum reinforcement ratio, ρ_{min}, adopted by Standards as

$$\rho_{\min} = \frac{\sigma_t}{6\Phi\gamma\sigma_y}, \tag{3}$$

with $\gamma = d/h$.

In the case of a *crushing failure*, the concrete matrix reaches its ultimate deformation, ε_{cu}, with steel reinforcement still within its elastic range. In this case, by means of the Bernoulli's hypothesis it is possible to state

$$\frac{\varepsilon_s}{\varepsilon_{cu}} = \frac{d-x}{x}. \tag{4}$$

Thus, the stress in steel may be found as

$$\sigma_s = \varepsilon_{cu}\left(\frac{d}{x} - 1\right)E_s. \tag{5}$$

Therefore, it is possible to find the depth of the neutral axis, x, by solving the following quadratic equation

$$\frac{\eta\sigma_c\beta b}{\varepsilon_{cu}E_sA_s}x^2 + x - d = 0. \tag{6}$$

Once the depth, x, of the neutral axis has been found, the ultimate bending moment, M_u, may be calculated as

$$M_u = \Phi\sigma_sA_s(d - 0.5x). \tag{7}$$

In this context, the *balanced failure* is defined as the failure mode at which concrete crushing and steel yielding simultaneously occur. The reinforcement ratio corresponding to this condition is defined *balanced reinforcement ratio*, ρ_{bal}. In a failure mode of this type, the depth of the neutral axis may be easily found from (5) as

$$x = \frac{\varepsilon_{cu}E_s}{\varepsilon_{cu}E_s + \sigma_y}d, \tag{8}$$

and the balanced reinforcement ratio, ρ_{bal}, may be defined as

$$\rho_{bal} = \frac{\gamma\eta\sigma_c\beta}{\sigma_y}\frac{\varepsilon_{cu}E_s}{\varepsilon_{cu}E_s + \sigma_y}. \tag{9}$$

In Fig. 4, the bearing capacity and the dimensionless neutral axis depth, x/d, of a RC beam ($h = 400$ mm) for different values of the reinforcement ratio are reported. The concrete matrix has a compression strength $\sigma_c = 35$ MPa, $\varepsilon_{cu} = 3.5$ ‰, $\beta = 0.8$, and $\eta = 0.85$. On the other hand, the steel yield strength is $\sigma_y = 500$ MPa, with $E_s = 2.1 \times 10^5$ MPa, and $d = 320$ mm. The two diagrams are obtained by means of (1, 2, 6, 7) by setting $\Phi = 1$. The balanced reinforcement ratio, ρ_{bal}, for this beam is $\rho_{bal} = 2.8\%$. Figure 4a shows that for $\rho < \rho_{bal}$ an increase in the reinforcement ratio leads to an almost linear increase in the load bearing capacity. On the other hand, for $\rho > \rho_{bal}$ only a small increase in M_u is recognised. This difference

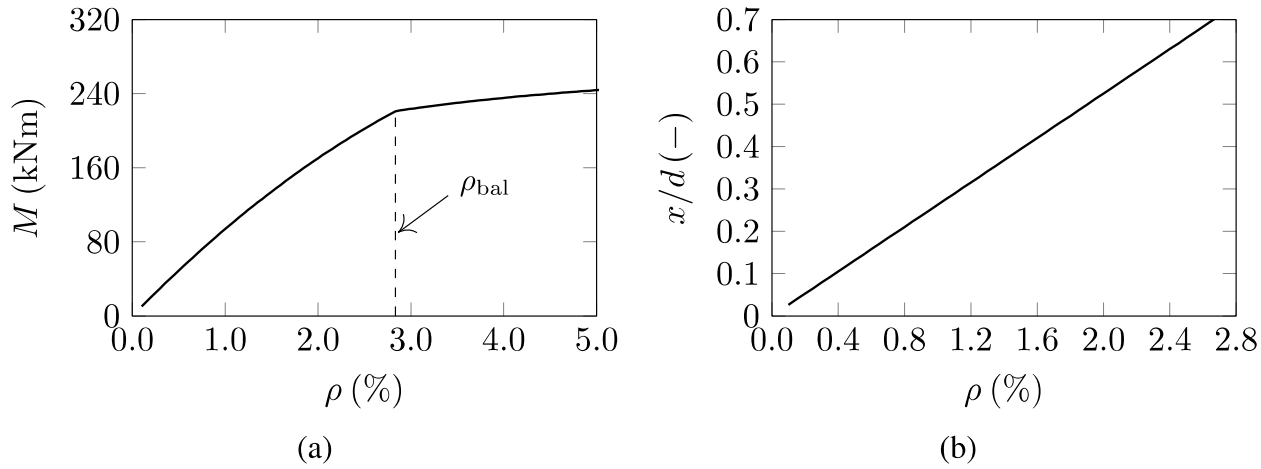

Fig. 4 Behaviour of a RC beam at ULS for increasing reinforcement ratios: (**a**) Bearing capacity; (**b**) Dimensionless neutral axis depth, *x/d*

in the response of the beam at ULS is due to a transition in the failure mechanism: if steel has a sufficient ductility, for $\rho < \rho_{bal}$ a flexural failure is obtained. On the other hand, for $\rho > \rho_{bal}$ a brittle catastrophic failure due to concrete crushing is detected without any plastic rotation capacity. This ductile-to-brittle transition is predicted by Standards by assuming a different strength reduction factor, Φ, for increasing reinforcement ratios, by defining an upper bound reinforcement limit, ρ_{max}, and/or by defining a maximum neutral axis depth (Fig. 4b).

The constitutive laws and the hypotheses introduced above form the Standards' theoretical background for beam design and assessment. On the other hand, they are not able to take into account the quasi-brittle nature of concrete, and size-scale effects in the transitions between failure mechanisms [5, 19, 20, 22, 25, 28] and on minimum and maximum reinforcement ratios.

In the past, important results in the study of size-scale effects on plain concrete beams in bending have been obtained by means of the Cohesive Crack Model [12, 26]. The Cohesive Crack Model is a Nonlinear Fracture Mechanics model that is able to describe the cracking process of concrete by taking into account the bridging effect of aggregates [10, 11]. In this model, a traditional σ-ε constitutive law is applied on the undamaged part of the beam until the tension strength, σ_t, is reached (Fig. 5a). Beyond this limit, strain-localization phenomena take place and a softening σ-w^t constitutive law is used, w^t being the crack opening displacement (Fig. 5b). In a cohesive crack it is possible to recognise two

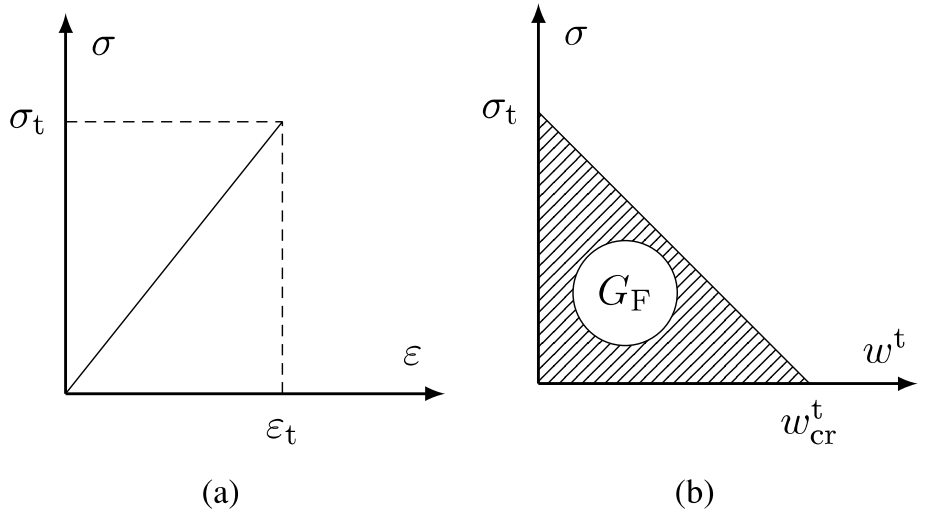

Fig. 5 Constitutive laws for the Cohesive Crack Model: (**a**) Pre-peak σ-ε law; (**b**) Post-peak σ-w^t relationship

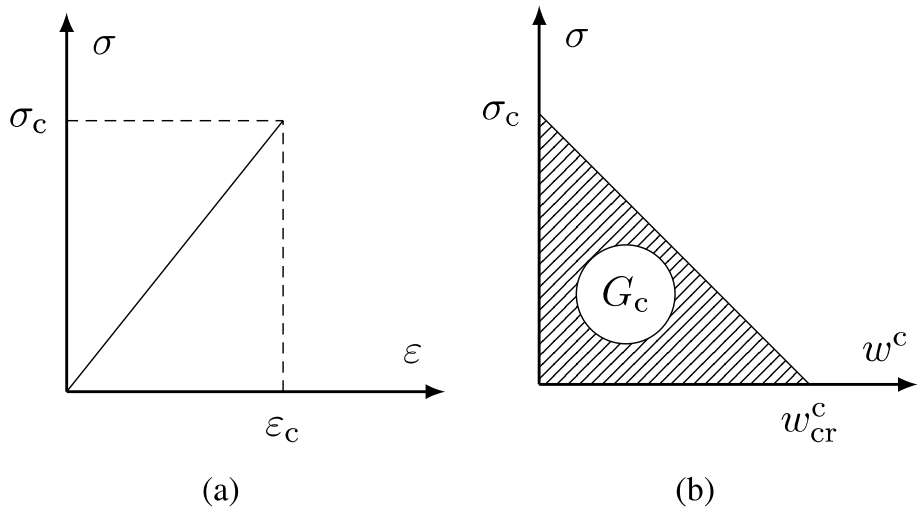

Fig. 6 Constitutive laws for the Overlapping Crack Model: (**a**) Pre-peak σ-ε law; (**b**) Post-peak σ-w^c relationship

different tips. The fictitious crack tip is the point where the tension strength is reached. On the other hand, the real crack tip is the point where the critical crack opening displacement, w^t_{cr}, is attained: beyond w^t_{cr} the crack faces are too far and the bridging effect of aggregates is null (Fig. 5b). The crack length included within the fictitious and the real crack tips form the process zone, where energy dissipation occurs. Parametric studies carried out by means of the Cohesive Crack Model [12] on plain concrete beams have demonstrated that a ductile-to-brittle transition is detected by increasing the concrete matrix tension strength, σ_t, and/or the beam depth, h, and/or by decreasing the fracture energy, G_F. This transition from a softening to snap-back post-peak behaviour has been widely confirmed by several experimental campaigns carried out in the past [7, 24].

In 1997, the International Union of Laboratories and Experts in Construction Materials, Systems and Structures (RILEM) organized a large experimental campaign [36] in order to study the effects of loading boundary conditions and specimen slenderness on the post-peak behaviour of concrete in compression. The results of this campaign have demonstrated that in the softening regime a reliable constitutive law for concrete in compression may be established only if a fictitious interpenetration, w^c, is considered. In this context, Carpinteri et al. [16] have introduced the Overlapping Crack Model to study strain-localization phenomena of concrete in compression. As in the Cohesive Crack Model, in the Overlapping Crack Model two different constitutive laws are applied. A first constitutive law defined in a traditional σ-ε diagram is used until the concrete compression strength, σ_c, is reached (Fig. 6a). On the other hand, beyond this limit a second constitutive law defined in a σ-w^c diagram is adopted (Fig. 6b). The area below the σ-w^c curve defines the concrete crushing energy, G_c, which has been demonstrated [27] to be a real property for concrete in compression.

Within the present paper, the Cohesive and the Overlapping Crack Models are coupled together in the Cohesive/Overlapping Crack Model (COCM). The COCM [1, 2, 14, 15, 17, 18] is able to study strain-localization phenomena in tension and compression, size-scale effects, and ductile-to-brittle transitions in RC and PC beams in a unified approach. Therefore, some parametric studies are presented in order to highlight the effects of the beam size-scale and reinforcement percentage on beam ductility. Moreover, Dimensional Analysis is used to determine the Brittleness Numbers that govern the ductile-to-brittle transitions in RC and PC beams. Thus, these Brittleness Numbers are used to identify a size-scale dependent minimum and a size-scale dependent maximum reinforcement percentage.

2 The Cohesive/Overlapping Crack Model

The Cohesive/Overlapping Crack Model (COCM) is able to describe cracking and crushing phenomena in RC or PC beams by means of an evolutionary analysis. More precisely, within this model the beam cross-section is discretized into n nodes, and at each computation step, t, the following equation is solved:

$$\{w\}^t = [K_F]\{F\}^t + [K_F]\{F_p\} + \{K_M\}M^t. \tag{10}$$

In (10), $\{w\}^t$ and $\{F\}^t$ are the vectors containing nodal openings/overlappings and forces at step t, respectively; $\{F_p\}$ is the vector of forces generated by a potential

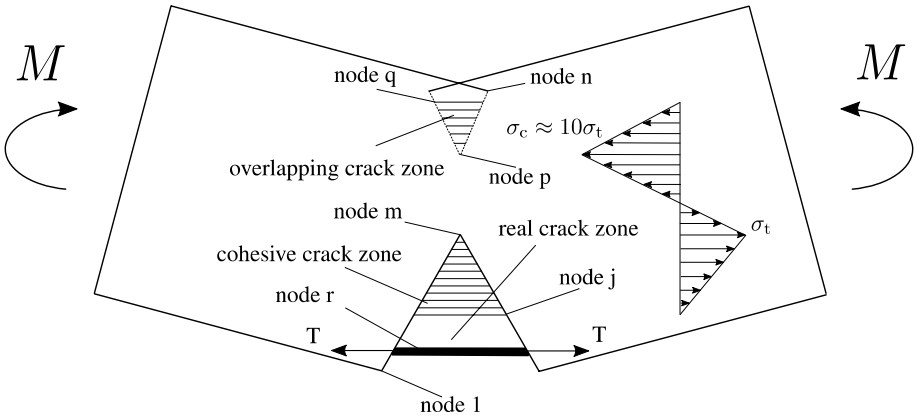

Fig. 7 Beam cross-section damaged in tension and compression at computation step *t*

compressive force due to prestressing; M^t is the bending moment at step *t*; $[K_F]$ and $\{K_M\}$ are the matrix and the vector containing nodal openings/overlappings for unit nodal forces and for a unit bending moment, respectively. The unknowns of (10) are $(2n+1)$ and are represented by the n nodal displacements $\{w\}^t$, the n nodal forces $\{F\}^t$, and by the applied bending moment, M^t. In order to reduce the number of the unknowns, in the general case of the damaged cross-section at step t of Fig. 7, it is possible to apply the Cohesive and the Overlapping constitutive laws of Figs. 5b and 6b to relate the nodal forces with the nodal displacements:

$$F_i^t = 0 \ \text{for}\, i = 1, \ldots, (j-1), i \neq r \tag{11a}$$

$$F_i^t = F_t\left(1 - \frac{w_i^t}{w_{cr}^t}\right) \ \text{for}\, i = j, \ldots, (m-1) \tag{11b}$$

$$w_i^t = 0 \ \text{for}\, i = m, \ldots, p \tag{11c}$$

$$F_i^t = -F_c\left(1 + \frac{w_i^t}{w_{cr}^c}\right) \ \text{for}\, i = (p+1), \ldots, q \tag{11d}$$

$$F_i^t = 0 \ \text{for}\, i = (q+1), \ldots, n \tag{11e}$$

$$F_i^t = f\left(w_i^t\right) \ \text{for}\, i = r \tag{11f}$$

j, m, p and q being the fictitious and real crack tip positions of the cohesive and overlapping zones as reported in Fig. 7; F_t is the tension force that triggers the cohesive zone propagation; F_c is the compressive force that triggers the overlapping zone propagation. The condition (11f) defines the crack closing force generated by reinforcement as a function of the nodal displacement w_r, where reinforcement is positioned. This force may be easily evaluated by means of bond-slip constitutive laws suggested by Model Code 2010 [21] as reported in Ruiz [32] and Cafarelli et al. [8]. Although the conditions (11) estabilish a relationship between nodal openings/overlappings and nodal forces, they do not allow the determination of M^t. In this framework, another constraint should be considered. More precisely, since the loading process of a RC beam may present snap-back and snap-through unstable branches, in the COCM the loading process is followed numerically by setting at each computation step an increased value of the crack depth by means of the Crack Length Control Scheme (CLCS) [6]. On the other hand, since in the COCM we have a crack in tension and a fictitious crack in compression (the overlapping zone), the CLCS should be extended to consider multi-cracking phenomena [9]. More precisely, if we assume that at step $(t–1)$ we have reached the convergence of the numerical procedure with a bending moment M^{t-1}, at step t the bending moment may be calculated as

$$M^t = M^{t-1} + \Delta M^t. \tag{12}$$

ΔM^t being a correction for M^{t-1} that should be applied to generate F_t in the fictitious cohesive crack tip, or F_c in the fictitious overlapping tip. In the general condition reported in Fig. 7, with a fictitious cohesive crack tip in m and a fictitious overlapping crack tip in p, two virtual corrections for M^{t-1} are calculated:

$$\Delta M_1^t = \frac{F_t - F_m(M^{t-1}+1)}{F_m\left(M^{t-1}+1\right) - F_m(M^{t-1})}, \tag{13a}$$

$$\Delta M_2^t = -\frac{F_c + F_p\left(M^{t-1}+1\right)}{F_p\left(M^{t-1}+1\right) - F_p\left(M^{t-1}\right)}, \tag{13b}$$

$F_m(M^{t-1}+1)$, $F_p(M^{t-1}+1)$ being the two forces generated in nodes m and p with a bending moment

Table 1 Mechanical and reinforcement ratio parameters of the experimental campaign carried out by Mansor et al. [29]

Beam	σ_c (MPa)	σ_t (MPa)	G_F (N/mm)	G_c (N/mm)	σ_y (MPa)	ρ (%)
R1	38.2	3.4	0.146	30.0	460	0.46
R2	37.5	3.4	0.145	30.0	459	0.75
R3	37.3	3.3	0.145	30.0	440	2.05
R4	37.0	3.3	0.145	30.0	460	0.69
R5	39.1	3.5	0.146	30.0	459	1.30
R6	40.7	3.5	0.147	30.9	440	3.00

$(M^{t-1}+1)$; $\mathrm{F}_m(M^{t-1})$, $\mathrm{F}_p(M^{t-1})$ being the two forces that we have in the same nodes with a bending moment equal to M^{t-1}. The real correction ΔM^t is set as

$$\Delta M^{\mathrm{t}} = \begin{cases} \Delta M_1^t \ \text{ if} \left|\Delta M_1^t\right| = \min\left(\left|\Delta M_1^t\right|, \left|\Delta M_2^t\right|\right) \\ \Delta M_2^{\mathrm{t}} \ \text{if} \left|\Delta M_2^t\right| = \min\left(\left|\Delta M_1^t\right|, \left|\Delta M_2^t\right|\right). \end{cases} \tag{14}$$

Once the value of M^{t} is calculated by means of (12, 13, 14), a check is performed on the displacements of the two process zones since according to the constitutive laws of Fig. 5b and Fig. 6b the following conditions should be ensured:

$$w_i^t \leq w_{\mathrm{cr}}^{\mathrm{t}} \ \text{ for } \ i = j, \ldots, (\mathrm{m}-1), \tag{15a}$$

$$w_i^t \geq -w_{\mathrm{cr}}^{\mathrm{c}} \ \text{ for } \ i = p+1, \ldots, q. \tag{15b}$$

If (15) are not satisfied, the two process zones are shrunk, the nodes j and q are moved, and the calculation of M^{t} is repeated. Therefore, the beam cross-section rotation, ϑ^t, is calculated by means of the Betti's Theorem as:

$$\vartheta^t = \{K_{\mathrm{M}}\}^{\mathrm{T}}\{F\}^t + D_{\mathrm{M}}M^t, \tag{16}$$

where D_{M} is the rotation generated by a unit bending moment. At the end of the current step t, if ΔM^t is calculated by means of (14a), the fictitious cohesive crack tip is moved in $(m+1)$. On the other hand, if ΔM^t is calculated by means of (14b), the fictitious overlapping crack tip is moved in $(p-1)$. Thus, the numerical algorithm moves to calculation step $(t+1)$ and all the procedure described above is repeated.

It is worth noting that (13) may be applied only if linear cohesive and overlapping constitutive laws are adopted: in the case that nonlinear laws are used, ΔM^t should be determinated by means of iterative methods. Moreover, it should be noted that the elastic coefficients of (10) and (16) may be calculated only once by means of a finite element software and then rescaled according to the particular beam geometry to be analysed.

The COCM is able to calculate the beam response in the bending moment-rotation (M-ϑ) diagram. On the other hand, the load-displacement (P-δ) curve may be easily obtained by following the procedure described in Mattock [30] and Cafarelli et al. [8].

3 Model validation

In this section, the COCM is validated by means of a numerical versus experimental comparison. More precisely, the experimental campaign carried out by Mansor et al. [29] is considered. The beams of this campaign have a width of 200 mm, a depth of 300 mm, and a reinforcement ratio, ρ, between 0.46%-3.00%, as reported in Table 1. The specimens were casted with a concrete matrix having a compression strength $\sigma_c > 35$ MPa, and with a steel reinforcement having a yield strength $\sigma_y > 400$ MPa. Since Mansor et al. [29] have not carried out experimental tests for the determination of concrete tension strength, σ_t, fracture energy, G_F, and crushing energy, G_c, the values of these parameters have been determinated according to Model Code 2010 [21] and the formula proposed by Suzuki et al. [35]. All the beams are tested in a four point bending scheme by using the applied load as loading parameter, as reported in Fig. 8.

In Fig. 9, the numerical (thick) and experimental (thin) curves are reported. It is possible to observe that the COCM provides results that are very close to the experimental ones. More precisely, the model is capable of describing in a reliable manner the ascending branch after concrete cracking and the plastic plateau generated by steel yielding. Moreover, the model proves to be able to predict the reduction of the plastic plateau, and the transition from a flexural to crushing failure by increasing the reinforcement percentage, ρ. In this context, it is important to note that all the numerical curves of Fig. 9 present a first snap-back branch after the first peak load and a second snap-back after the plastic plateau. These instabilities are respectively triggered by concrete cracking and concrete crushing and are absent in the experimental curves due to the adopted loading parameter.

Althought the experimental campaign of Mansor et al. [29] was planned to study the ductility of RC beams, it completely disregards size-scale effects. In order to recover this lack, in the next two sections of the paper

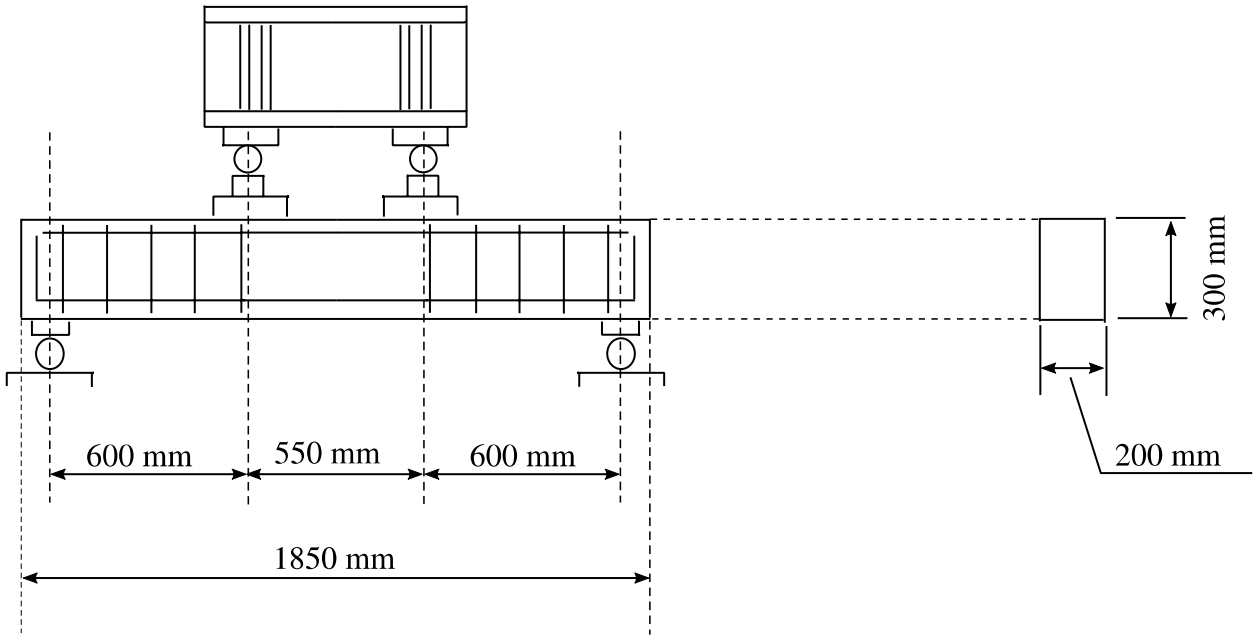

Fig. 8 Beam geometry and loading conditions adopted by Mansor et al. [29]

some parametric studies carried out by means of the COCM are presented.

4 Failure-mode scale-transitions in RC beams

In Fig. 10, a numerical investigation on RC beams performed by means of the COCM is reported. The study considers four different reinforcement ratios, ρ, between 0.5% and 3.0%. Moreover, for each reinforcement percentage, seven different beam depths, h, between 0.1 m and 2.0 m are considered. The beam thickness, b, is fixed in order to have a ratio $h/b=2$, and the reinforcement position is set in order to have $d=0.9\ h$. The concrete matrix has the following properties: $\sigma_c=40$ MPa; $G_c=30$ N/mm; $\sigma_t=4$ MPa; $G_F=0.08$ N/mm. On the other hand, the steel has a yield strength $\sigma_y=400$ MPa. In Fig. 10a, the curves for $\rho=0.5\%$ are reported. It may be observed that for this reinforcement percentage the beam having $h=0.1$ m has a large plastic rotation capacity. However, a clear reduction in the width of the plastic plateau by increasing the beam depth, h, may be detected. In Fig. 10b the case of $\rho=1.0\%$ is analysed. For this reinforcement ratio, all the beams with $h\leq 1.0$ m present a failure mode governed by steel yielding, and all the beams with $h>1.0$ m exhibit concrete crushing without any rotation capacity. In this framework, for this reinforcement percentage a ductile-to-brittle transition is detected for $h=1.0$ m.

In Fig. 10c, the curves for $\rho=2.0\%$ are reported. As in the previous cases, the width of the plastic plateau is reduced by increasing the beam depth, h. However, for this higher reinforcement ratio a flexural to crushing failure transition is obtained for a lower beam depth: for $h=0.6$ m, only a small plastic plateau may be recognised. By increasing further the reinforcement ratio (Fig. 10d), all the investigated beams migrate to a completely catastrophic behaviour: after the peak load, very steep snap-back instabilities triggered by concrete crushing are revealed and a null rotation capacity is detected.

5 Failure-mode scale-transitions in PC beams

Several experimental campaigns on PC beams carried out in the past were designed on small scale specimens in order to comply with laboratory constraints, and few studies exist on size-scale effects on these structural elements [37]. Thus, as in the case of RC beams, in this section of the paper a numerical investigation on these elements by means of the COCM is presented.

The parametric analysis is carried out considering four different prestressing reinforcement percentages, ρ_p, in the range 0.1%-0.8%. The concrete matrix has the same mechanical parameters of the numerical investigation of the previous section, and the steel yield strength is fixed to $\sigma_y=1700$ MPa. The study considers five different beam depths, h, in the range 0.4 m-1.5 m. In Fig. 11, the obtained numerical curves are reported. It may be observed that for low reinforcement percentages (Fig. 11a, b) the behaviour of PC beams is similar to that of RC beams: after concrete cracking, an ascending branch up to steel yielding is recognised. After steel yielding, a plastic plateau is described, and at the end

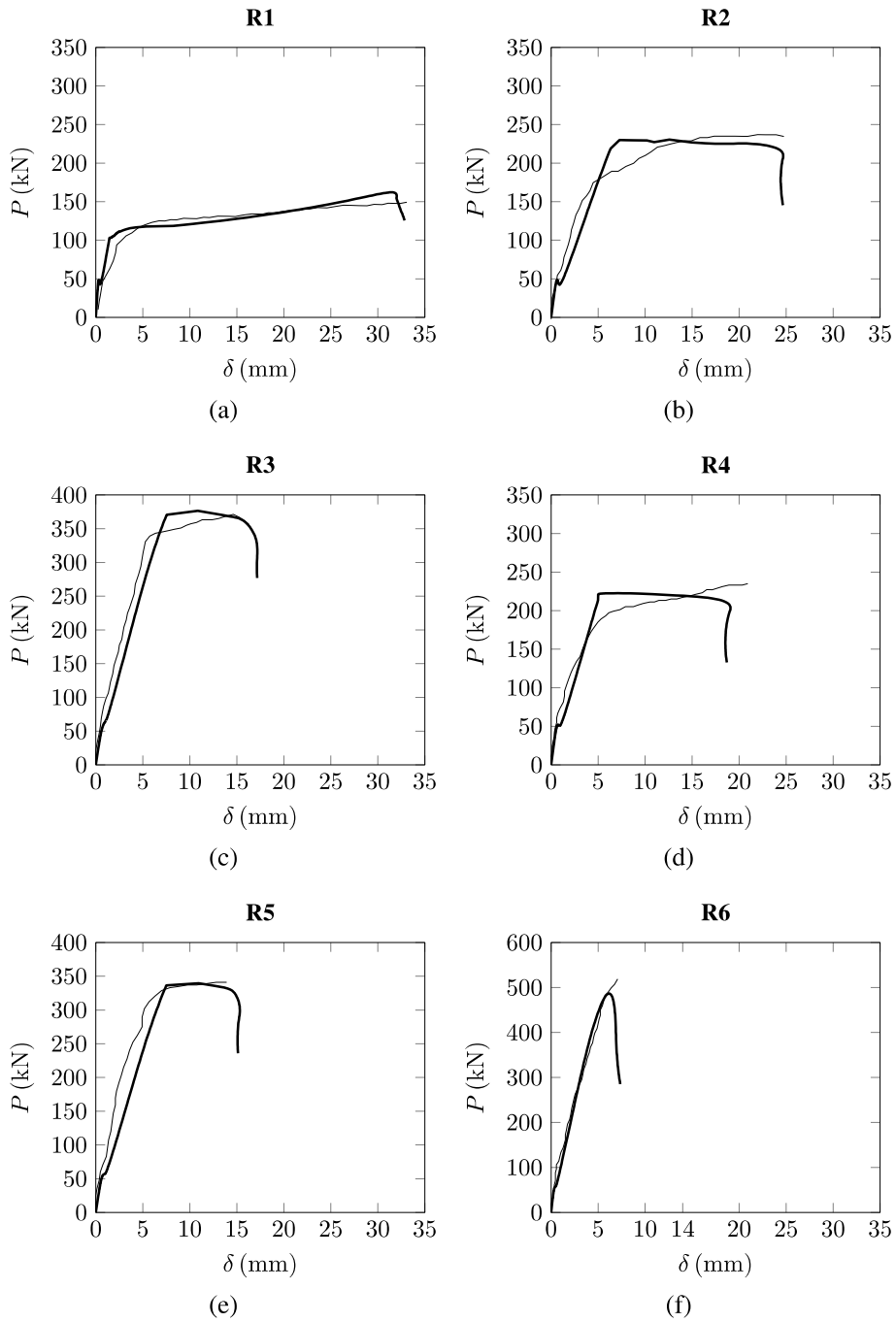

Fig. 9 Comparison between numerical (thick) and experimental (thin) results: (**a**) $\rho = 0.46\%$; (**b**) $\rho = 0.75\%$; (**c**) $\rho = 2.05\%$; (**d**) $\rho = 0.69\%$; (**e**) $\rho = 1.30\%$; (**f**) $\rho = 3.00\%$

of this plastic plateau a snap-back instability triggered by concrete crushing is detected. In this framework, the beams having $\rho_p = 0.1\%$ and $\rho_p = 0.2\%$ have a stable behaviour since the ULS is reached with yielded steel. However, it may also be recognised that the width of the plastic plateau is reduced by increasing the beam depth, clearly suggesting size-scale effects. In Fig. 11c, the curves obtained for $\rho_p = 0.4\%$ are reported. For this reinforcement percentage, all the investigated beam depths present unstable concrete compression failure: after concrete cracking, the peak load is reached, and unstable strain localization phenomena are triggered without

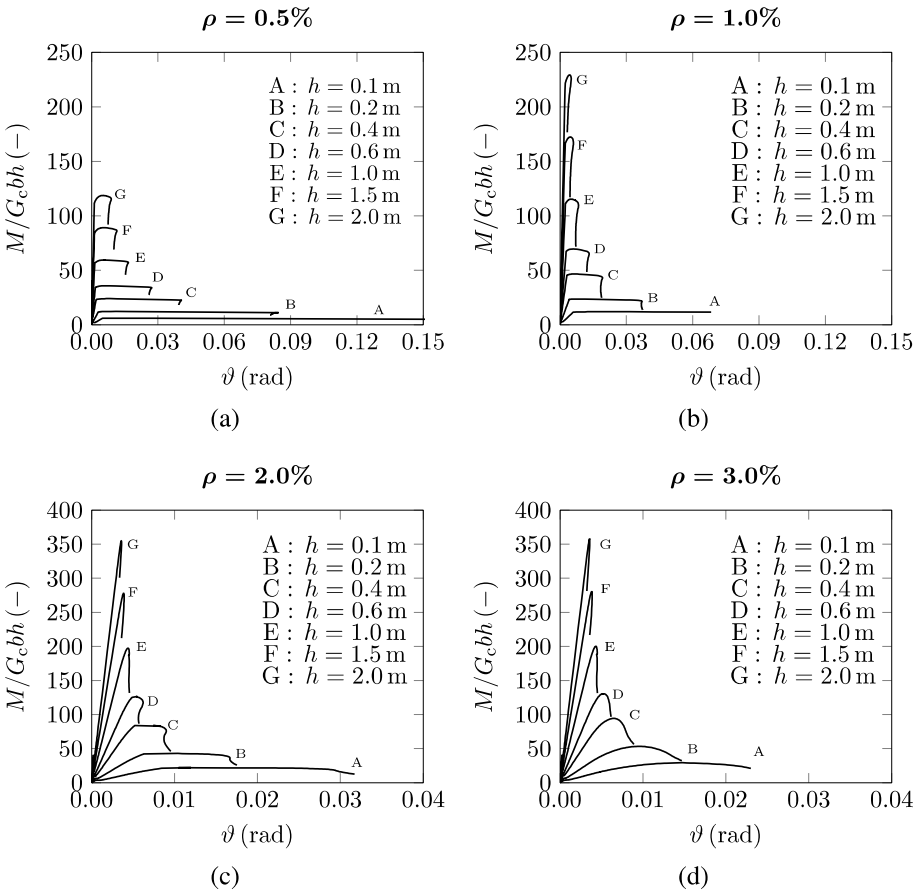

Fig. 10 Size-scale effects on RC beams for different reinforcement ratios, ρ

steel yielding. This behaviour is confirmed by Fig. 11d where the reinforcement percentage $\rho_p = 0.8\%$ is analysed. For this higher reinforcement ratio, the post-peak behaviour of the beams is characterized by steeper snap-back branches, suggesting the more severe crushing of concrete.

6 Dimensional Analysis and Brittleness Numbers

Dimensional Analysis [4, 13] might be used in the investigation of the different failure modes of RC structures, since it is able to reveal the geometrical and mechanical characteristics affecting the ductile-to-brittle transitions. In particular, the behaviour of a RC beam in bending may be written as:

$$\mathrm{F}\left(\sigma_t, K_{IC}, \sigma_c, G_c, F_b, F_e, h; \frac{\ell}{h}, \frac{b}{h}\right) = 0, \tag{17}$$

K_{IC} being the concrete toughness; F_b the maximum bridging force exerted by reinforcement; F_e the force generated at beam extrados due to prestressing; ℓ the beams span; b the beam thickness. If we are interested in the investigation of the flexural failure of RC elements, we may neglect σ_c, G_c, and F_e, leading to a simplification of this general relationship:

$$\mathrm{F}_1\left(\sigma_t, K_{IC}, F_b, h; \frac{\ell}{h}, \frac{b}{h}\right) = 0. \tag{18}$$

We may further reduce the dimension of the problem stated in (18) by adopting h and K_{IC} as independent variables

$$\Pi_1\left(\frac{K_{IC}}{\sigma_t h^{0.5}}, \frac{F_b}{K_{IC} h^{1.5}}; \frac{\ell}{h}, \frac{b}{h}\right) = 0. \tag{19}$$

In (19) it is possible to recognise the *Tension Matrix Brittleness Number*,

$$s_t = \frac{K_{IC}}{\sigma_t h^{0.5}}, \tag{20}$$

and the *Lower Limit Reinforcement Brittleness Number*

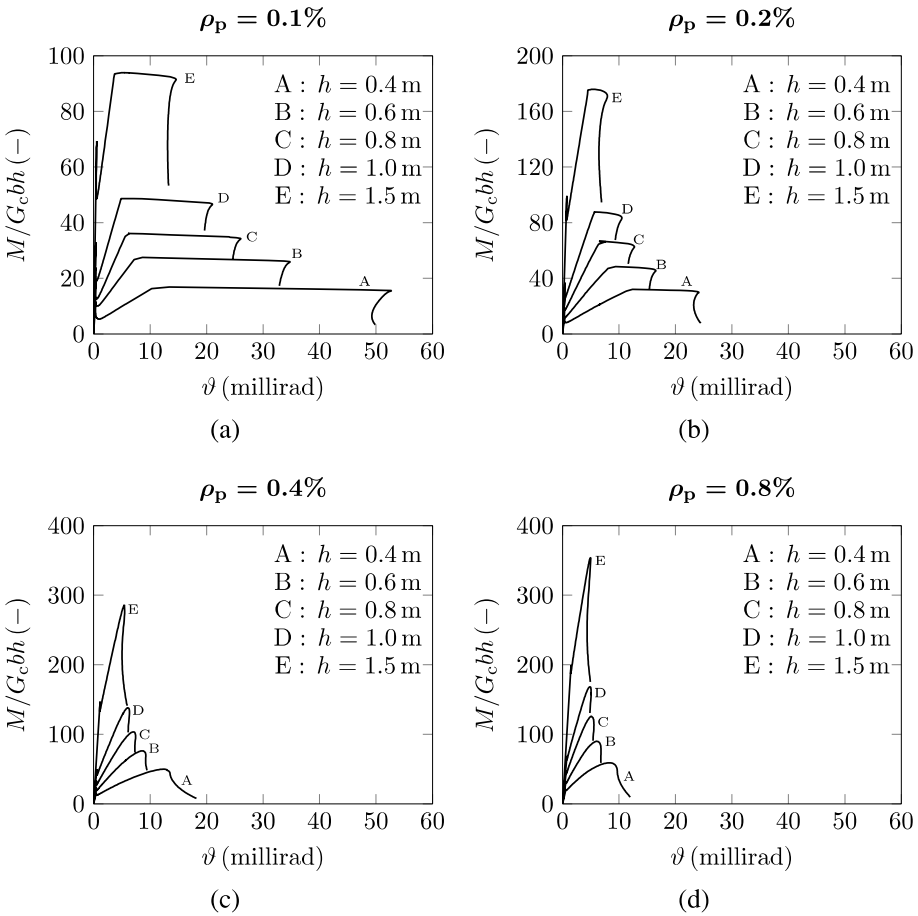

Fig. 11 Size-scale effects on PC beams for different prestressing reinforcement ratios, ρ_p

$$N_P^L = \frac{F_b}{K_{IC} h^{1.5}} \propto \rho \frac{\sigma_b h^{0.5}}{K_{IC}}. \tag{21}$$

On the other hand, if we want to study the crushing failure of PC beams, σ_t and K_{IC} may be neglected in (17). Therefore, the problem is reduced to:

$$F_2\left(\sigma_c, G_c, F_b, F_e, h; \frac{\ell}{h}, \frac{b}{h}\right) = 0. \tag{22}$$

In this case, if $(G_c E)^{0.5}$ and h are assumed as independent parameters, (22) may be simplified as:

$$\Pi_2\left(\frac{\sqrt{G_c E}}{\sigma_c h^{0.5}}, \frac{F_b}{\sqrt{G_c E} h^{1.5}}, \frac{F_e}{\sqrt{G_c E} h^{1.5}}; \frac{\ell}{h}, \frac{b}{h}\right) = 0, \tag{23}$$

where it is possible to recognise the *Compression Matrix Brittleness Number*

$$s_c = \frac{\sqrt{G_c E}}{\sigma_c h^{0.5}}, \tag{24}$$

the *Upper Limit Reinforcement Brittleness Number*

$$N_P^U = \frac{F_b}{\sqrt{G_c E} h^{1.5}} \propto \rho \frac{\sigma_b h^{0.5}}{\sqrt{G_c E}}, \tag{25}$$

and the *Prestressing Reinforcement Brittleness Number*

$$N_P^p = \frac{F_e}{\sqrt{G_c E} h^{1.5}} \propto \rho \frac{\sigma_p h^{0.5}}{\sqrt{G_c E}} (6e/h - 1), \tag{26}$$

σ_p being the prestressing stress, and e being the tendon eccentricity.

7 Size-scale dependent minimum and maximum reinforcement percentages

The Dimensional Analysis presented in the previous section demonstrates that the flexural failure of RC beams is influenced by the two Brittleness Numbers s_t, N^L_P, and that the crushing failure is influenced by the other two Brittleness Numbers s_c, N^U_P. In this framework, since the COCM is able to predict the flexural to crushing failure mode transitions by increasing the

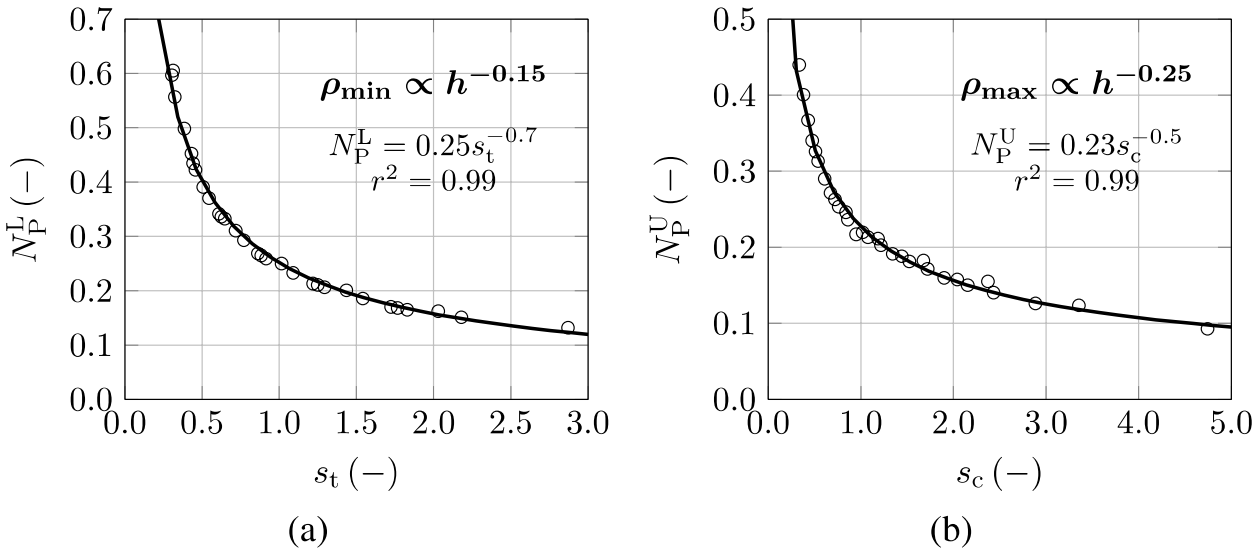

Fig. 12 Size-scale dependent reinforcement limits in RC beams: (**a**) Lower limit; (**b**) Upper limit

reinforcement percentage, ρ, and/or the beam size-scale, h, it may be adopted to outline size-scale dependent minimum, ρ_{min}, and maximum, ρ_{max}, reinforcement percentages. The numerical investigation presented in the following has been set considering several concrete grades in the range 20–80 MPa. For each concrete grade, several beam size-scales in the range 0.1–6.4 m have been analysed, and for each beam depth the reinforcement ratio has been increased progressively. More precisely, the minimum reinforcement ratio, ρ_{min}, has been calculated as the reinforcement ratio that is able to generate an ultimate bending moment equal to the cracking bending moment. Whereas, the maximum reinforcement percentage, ρ_{max}, has been calculated as the minimum reinforcement ratio that is able to trigger concrete crushing before steel yielding. The results of this study are presented in Fig. 12 for RC beams and in Fig. 13 for PC beams, where two values of the Brittleness Number N^P_P are considered. In this context, the

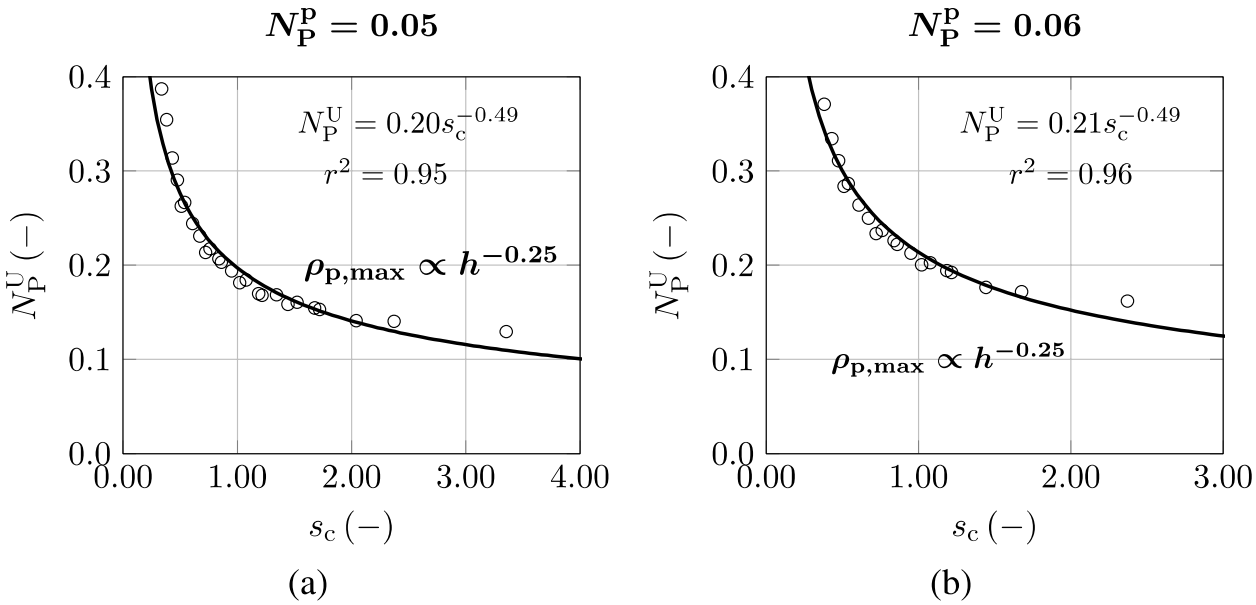

Fig. 13 Size-scale dependent upper reinforcement limit for PC beams: (**a**) $N_P^P = 0.05$; (**b**) $N_P^P = 0.06$

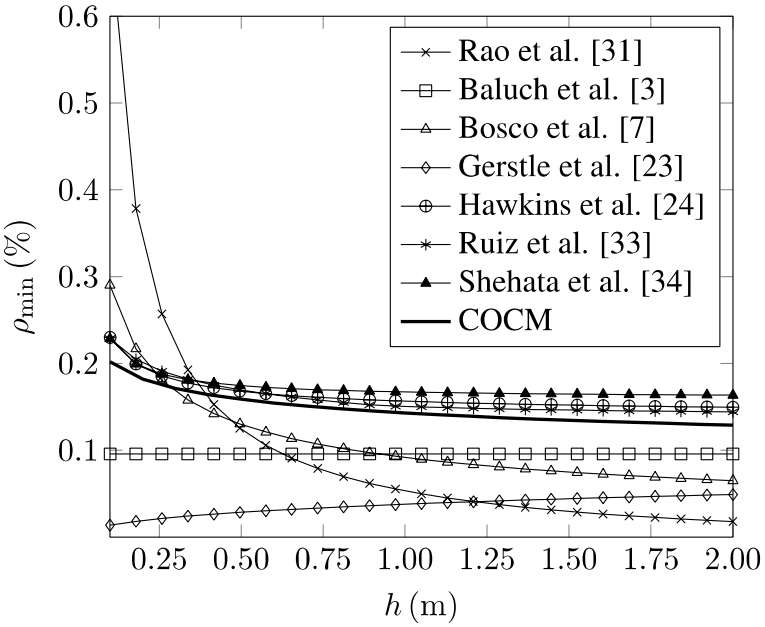

Fig. 14 Minimum reinforcement comparison

COCM reveals a variation of $\rho_{\min}$ proportional to $h^{-0.15}$, and a variation of $\rho_{\max}$ proportional to $h^{-0.25}$.

In the past several models [3, 7, 23, 24, 31, 33, 34] have been proposed to determine an effective minimum reinforcement percentage for RC beams. Some of the size-scale laws for $\rho_{\min}$ found in literature are compared in Fig. 14 together with the size-scale law found by means of the COCM. It is possible to observe that all the models predict a reduction of $\rho_{\min}$ by increasing the beam size-scale, h, with the only exception of the Gerstle's model [23].

8 Conclusion

The Cohesive/Overlapping Crack Model (COCM) is a Nonlinear Fracture Mechanics model that is able to simulate strain localization phenomena occurring in RC structures by adopting constitutive laws for the concrete matrix defined in a stress-displacement diagram. Fracture Mechanics and experimental tests carried out in the past have demonstrated that only this type of law is able to predict the ductile-to-brittle transitions occurring in concrete and reinforced concrete specimens in a comprehensive manner. On the other hand, constitutive laws and calculation models currently included in Standards are still based on traditional σ-ε approaches, demonstrating their inability in predicting the above-mentioned phenomena. In this paper, the COCM together with Dimensional Analysis has been adopted to define minimum and maximum size-scale dependent reinforcement ratios, providing the limits in which RC beams may exhibit a stable behaviour. The outcomes within the present paper may have important consequences on structural design, structural assessment and retrofitting, and may be used to better understand the mechanical behaviour of new concrete composites made of high strength concrete mixtures, fibres, fibre reinforcing polymer bars (FRP), and recycled aggregates.

Authors' contributions

Renato Cafarelli: Conceptualization, Formal analysis, Data curation, Software, Visualization, Writing – original draft.
Federico Accornero: Conceptualization, Formal analysis, Methodology, Supervision, Validation, Writing – original draft.
Alberto Carpinteri: Conceptualization, Formal analysis, Methodology, Supervision, Validation, Writing – review & editing.

Funding

Federico Accornero acknowledges the support from STU Outstanding Talent Grant N. 140-09423016.

Availability of data and materials

The data that support the findings of this study are available from the corresponding author upon reasonable request.

Declarations

Competing interests

Federico Accornero and Alberto Carpinteri are editorial board members for Smart Construction and Sustainable Cities and were not involved in the editorial review, or the decision to publish, this article. All authors declare that there are no other competing interests.

Received: 1 September 2023 Revised: 14 January 2024 Accepted: 16 January 2024
Published online: 18 March 2024

References

1. Accornero F, Cafarelli R, Carpinteri A (2021) Cracking and crushing in prestressed concrete beams. Struct J 118(2):101–109. https://doi.org/10.14359/51728184
2. Accornero F, Cafarelli R, Carpinteri A (2022) The cohesive/overlapping crack model for plain and RC beams: scale effects on cracking and crushing failure. Mag Concr Res 74(9):433–450. https://doi.org/10.1680/jmacr.20.00260
3. Baluch MH, Azad AK, Ashmawi W (1992) Fracture mechanics application to reinforced concrete members in flexure. In: Carpinteri A (ed) Application of Fracture Mechanics to Reinforced Concrete, 1st edn. CRC Press, London, pp 413–436
4. Barenblatt GI (2003) Scaling. Cambridge texts in applied mathematics. Cambridge University Press, Cambridge
5. Bigaj A, Walraven J (2002) Size effects in plastic hinges of reinforced concrete members. Heron 47(1):53–75
6. Bocca P, Carpinteri A, Valente S (1990) Size effects in the mixed mode crack propagation: softening and snap-back analysis. Eng Fract Mech 35(1–3):159–170. https://doi.org/10.1016/0013-7944(90)90193-K
7. Bosco C, Carpinteri A (1999) Fracture mechanics evaluation of minimum reinforcement in concrete structures. In: Carpinteri A (ed) Application of Fracture Mechanics to Reinforced Concrete, 1st edn. CRC Press, London, pp 347–377
8. Cafarelli R, Accornero F, Carpinteri A (2023) Size-scale effects in high-performance reinforced and prestressed concrete T-beams. Struct Concr 24(5):5649–5663. https://doi.org/10.1002/suco.202200673
9. Cafarelli R, Accornero F, Carpinteri A (2024) Snap-back analysis of fracture evolution in multi-cracked masonry arches. In: Gabriele S, Manuello Bertetto A, Marmo F, Micheletti A (eds) Shell and Spatial Structures, Proceedings of IWSS 2023, 1st edn. Springer, Switzerland, pp. 80–87. https://doi.org/10.1007/978-3-031-44328-2_9
10. Carpinteri A (1981) A fracture mechanics model for reinforced concrete collapse. IABSE reports of the working commissions 34:18–30. https://doi.org/10.5169/seals-26877
11. Carpinteri A (1984) Stability of fracturing process in RC beams. J Struct Eng 110(3):544–558. https://doi.org/10.1061/(ASCE)0733-9445(1984)110:3(544)
12. Carpinteri A (1989) Cusp catastrophe interpretation of fracture instability. J Mech Phys Solids 37(5):567–582. https://doi.org/10.1016/0022-5096(89)90029-X
13. Carpinteri A, Accornero F (2021) Dimensional analysis of critical phenomena: self-weight failure, turbulence, resonance, fracture. Phys Mesomech 24:459–463. https://doi.org/10.1134/S102995992104010X
14. Carpinteri A, Accornero F, Cafarelli R (2021) Scale-dependent maximum reinforcement percentage in reinforced concrete beams. Struct Concr 22(4):2155–2166. https://doi.org/10.1002/suco.202000573
15. Carpinteri A, Accornero F, Cafarelli R (2022) Scale effects in prestressed concrete structures: Maximum reinforcement percentage to avoid brittle crushing. Eng Struct 255:113911. https://doi.org/10.1016/j.engstruct.2022.113911
16. Carpinteri A, Corrado M, Mancini G, Paggi M (2008) The overlapping crack model for uniaxial and eccentric concrete compression tests. Mag Concr Res 61(9):745–757. https://doi.org/10.1680/macr.2008.61.9.745
17. Carpinteri A, Corrado M, Mancini G, Paggi M (2009) Size-scale effects on plastic rotational capacity of reinforced concrete beams. Struct J 106(6):887–896. https://doi.org/10.14359/51663190
18. Carpinteri A, Corrado M, Paggi M, Mancini G (2009) New model for the analysis of size-scale effects on the ductility of reinforced concrete elements in bending. J Eng Mech 135(3):221–229. https://doi.org/10.1061/(ASCE)0733-9399(2009)135:3(221)
19. Cohn MZ (1979) Inelasticity of reinforced concrete and structural standards. J Struct Div 105(11):2221–2241. https://doi.org/10.1061/JSDEAG.000527
20. Cosenza E, Greco C, Manfredi G (1991) Theoretical evaluation of inelastic rotations and displacements in the reinforced concrete monodimensional elements. Atti dell' Accademia Nazionale Dei Lincei 2:249–258
21. fib (Fédération International du Béton) (2013) Model Code for Concrete Structures 2010. John Wiley & Sons, New York
22. fib Bulletin (1998) Ductility of reinforced concrete structures Sprint Druck Stuttgart. p 242
23. Gerstle WH, Dey PP, Prasad NNV, Rahulkumar P, Xie M (1992) Crack growth in flexural members – a fracture mechanics approach. Struct J 89(6):617–625. https://doi.org/10.14359/4132
24. Hawkins NM, Hjorteset K (1999) Minimum reinforcement requirements for concrete flexural elements. In: Carpinteri A (ed) Application of Fracture Mechanics to Reinforced Concrete, 1st edn. CRC Press, London, pp 379–412
25. Hillerborg A (1990) Fracture mechanics concepts applied to moment capacity and rotational capacity of reinforced concrete beams. Eng Fract Mech 35(1–3):233–240. https://doi.org/10.1016/0013-7944(90)90201-Q
26. Hillerborg A, Modéer M, Petersson P-E (1976) Analysis of crack formation and crack growth in concrete by means of fracture mechanics and finite elements. Cem Concr Res 6(6):773–781. https://doi.org/10.1016/0008-8846(76)90007-7
27. Jansen DC, Shah S (1997) Effect of length on compressive strain softening of concrete. J Eng Mech 123(1):25–35. https://doi.org/10.1061/(ASCE)0733-9399(1997)123:1(25)
28. Leonhardt F (1965) Reducing the shear reinforcement in reinforced concrete beams and slabs. Mag Concr Res 17(53):187–198. https://doi.org/10.1680/macr.1965.17.53.187
29. Mansor AA, Mohammed AS, Salman WD (2020). Effect of longitudinal steel reinforcement ratio on deflection and ductility in reinforced concrete beams. IOP Conference Series: Material Science and Engineering 888:012008. https://doi.org/10.1088/1757-899X/888/1/012008
30. Mattock AH (1965) Rotational capacity of hinging regions in reinforced concrete beams. Struct J 12:143–181. https://doi.org/10.14359/16716
31. Rao GA, Aravind J, Eligehausen R (2007) Evaluation of minimum flexural reinforcement in RC beams. J Struct Eng 34:277–283
32. Ruiz G (2001) Propagation of a cohesive crack crossing a reinforcement layer. Int J Fract 111:265–282. https://doi.org/10.1023/A:1012260410704
33. Ruiz G, Elices M, Planas J (1999) Size effect and bond-slip dependence of lightly reinforced concrete beams. In: Carpinteri A (ed) Minimum reinforcement in concrete members, 1st edn. Elsevier, pp 67–97
34. Shehata IAEM, Shehata LCD, Garcia SLG (2002) Minimum steel ratios in reinforced concrete beams made of concrete with different strengths – theoretical approach. Mater Struct 36:3–11. https://doi.org/10.1007/BF02481565
35. Suzuki M, Matsuzaki Akiyama M, H, Dang, TH, (2006) Concentric loading tests of RC columns with normal and high-strength materials and averaged stress-strain model for confined concrete considering compressive fracture energy. Naples, Italy, Second International fib Congress
36. van Mier JGM et al (1997) Strain-softening of concrete in uniaxial compression. Mater Struct 30:195–209. https://doi.org/10.1007/BF02486177
37. Vorel J, Gattu M, Bažant Z (2014) Size effect in flexure of prestressed concrete beams failing by compression softening. J Struct Eng 140(10):04014068. https://doi.org/10.1061/(ASCE)ST.1943-541X.0000983
38. Whitney CS (1937) Design of reinforced concrete members under flexure or combined flexure and direct compression. Struct J 33(3):483–498. https://doi.org/10.14359/8429

Publisher's Note

Springer Nature remains neutral with regard to jurisdictional claims in published maps and institutional affiliations.